Engineering of Metal–Organic Frameworks/Gelatin Hydrogel Composites Mediated by the Coacervation Process for the Capture of Acetic Acid

Subharanjan Biswas, Mohamed Haouas, Cátia Freitas, Carla Vieira Soares, Abeer Al Mohtar, Ali Saad, Heng Zhao, Georges Mouchaham, Carine Livage, Florent Carn, et al.

Engineering of Metal-Organic-Frameworks/Gelatin Hydrogel Composites Mediated by the Coacervation Process for the Capture of Acetic Acid

Subharanjan Biswas,[a] Mohamed Haouas,[a] Cátia Freitas,[b] Carla Vieira-Soares,[c] Abeer Al Mohtar,[b] Ali Saad,[a] Heng Zhao,[d] Georges Mouchaham, Carine Livage,[a] Florent Carn,[e] Nicolas Menguy,[f] Guillaume Maurin,[c] Moises L. Pinto,[b] and Nathalie Steunou.*[a,d]

[a.] Institut Lavoisier de Versailles, UMR CNRS 8180, Université de Versailles St Quentin en Yvelines, Université Paris Saclay, Versailles, France.
[b.] CERENA, Departamento de Engenharia Química, Instituto Superior Técnico, Universidade de Lisboa, 1049-001 Lisboa, Portugal.
[c.] Institut Charles Gerhardt Montpellier, UMR 5253 CNRS, Université de Montpellier, Montpellier, France.
[d.] Institut des Matériaux Poreux de Paris, UMR 8004 CNRS-ENS-ESPCI, PSL research university, Paris, France.
[e.] Laboratoire Matière et Systèmes Complexes, UMR CNRS 7057, Université Paris Diderot, Bât. Condorcet, Paris, France.
[f.] Sorbonne Université, UMR CNRS 7590, MNHN, IRD, Institut de Minéralogie de Physique des Matériaux et de Cosmochimie, IMPMC, Paris, France.

A novel strategy is proposed to synthesize MOF-gelatin bionanocomposites by taking profit of the thermo-reversible character of gelatin and the liquid-liquid phase separation process (i.e. coacervation). This allows the formation of bionanocomposites based on the series of Zr^{4+} dicarboxylate MOF (UiO-66 and MOF-801) differing by their hydrophilic-hydrophobic balance and their chemical functionality. Bionanocomposites with homogeneous and uniform distribution of MOF particles in gelatin matrix as well as a high MOF loading (as high as 90%) without compromising their porosity were prepared as a result of an excellent physico-chemical matching between MOFs and gelatin. Finally, this series of bionanocomposites were shaped into films or monoliths and have shown a high performance for the selective adsorption of acetic acid in presence of humidity. These materials can be regarded as highly efficient adsorbents for cultural heritage preservation.

Introduction

Metal-organic frameworks (MOFs), a class of porous and crystalline hybrid materials, composed of metal ions and organic polydentate ligands have sparked tremendous research interests due to their highly ordered pore structure, high internal surface areas and chemical functionality.[i,ii] These unique properties make these materials very promising for a wide range of applications including gas storage and separation,[iii] sensing, catalysis, biomedicine [iv,v] and energy storage.[vi] However, MOFs present several shortcomings that still limits their transfer and implementation in real industrial applications to a great extent. Above all, numerous MOFs have shown a limited chemical and thermal stability.[vii] In particular, their low water stability can induce an irreversible degradation of their structure upon exposure to humid air for a few hours. Moreover, typical MOF syntheses generally produce brittle and insoluble powdered materials. The intrinsic fragility of MOF powders and their known poor processability and handling as well as low mass/heat transfer rate along with high pressure drop when being piled strongly hampers the potential of developing applications by using MOFs.[viii] To date, MOFs have been mainly processed in the forms of pellets, granules, beads, fibers and membranes but in many cases, the accessibility to the MOF porosity is lost after shaping.**Erreur ! Signet non défini.** This issue was mainly addressed through the integration of MOFs with diverse supporting materials such as carbon-based materials (polymers, carbon nanotubes, graphene, graphene oxide, textile fibers)[ix,x,xi,xii,xiii,xiv] or metal oxides,[xv] thereby leading to multifunctional composites with a synergistic combination of the properties of MOFs (porosity, crystallinity) and the supporting matrix (mechanical stability, processability). Moreover, this strategy can also be efficient to impart novel functionalities such as enhanced stability and electron conductivity or extend the porosity of MOFs in the meso- or macroporous regime.**Erreur ! Signet non défini.-Erreur ! Signet non défini.** This hybridization of MOFs with carbon-based materials or oxides led to a wide diversity of composites used in many applications including gas adsorption and separation, sensing, water purification, biotechnology.**Erreur ! Signet non défini.-Erreur ! Signet non défini.** However, these composites suffer frequently from a strong aggregation of MOF particles as a result of a poor interfacial compatibility between the MOF and the host matrix.**Erreur ! Signet non défini.,Erreur ! Signet non défini.** In particular, this MOF particle agglomeration is a recurrent phenomenon reported for composites prepared by blending polymer or graphene oxide host matrices with preformed MOF particles.**Erreur ! Signet non défini.** This issue becomes even more critical at higher MOF loadings that are usually required to optimize the performance
of composites. Therefore, various alternative strategies have been explored to enhance the physico-chemical matching between MOF and carbon based materials and thus to prepare homogeneous shaped composites without losing the porosity of MOFs. These approaches include the surface modification of MOFs,[xvi] the covalent grafting of polymers onto the outer surface of MOF particles,**Erreur ! Signet non défini.,**[xvii,xviii] the in situ formation of MOF within the polymer matrix,[xix] the in situ polymerization of polymers,[xx,xxi] polymers templating MOF growth**Erreur ! Signet non défini.**

and the synthesis of MOFs using polymer ligands (polyMOF)[xxii]. However, numerous MOF-polymer composites still present significant shortcomings such as low surface area as a result of the MOF pore clogging by polymer chains or a poor distribution of MOFs particles in the polymer matrix. In addition, the preparation of these composite implies time-consuming multi-step synthetic procedures and the use of synthetic polymers that are derived from petrochemical products can led to serious toxicity, environmental and health concerns.

This work aims to report a novel and simple strategy for the synthesis of hydrogel composites combining gelatin and a series of the Zr^{4+} dicarboxylate MOF with the UiO-66 (UiO= University of Oslo) type structure bearing different functional organic linkers.[xxiii] Gelatin is one of the most commonly used protein biopolymer in industry for drugs and cosmetics microencapsulation due to its low cost, biodegradability, nontoxicity and renewability.[xxiv] Its combination with a wide range of inorganic materials including (hydr)oxides, hydroxyapatite, clays, zeolites and metals was mainly explored to reinforce the mechanical properties of gelatin in tissue engineering or design multifunctional biohybrid materials for regenerative medicine, drug vectorization or biosensing.[xxv,xxvi] Moreover, gelatin could exert a remarkable level of control over the nucleation and growth of biogenic inorganic materials such as fluoroapatite mesocrystals.[xxvii] Such ability of gelatin for morphogenesis in soft conditions was mainly ascribed to its self-organization properties into triple helices and the existence of attractive interactions at the fluoroapatite/gelatin interface. In contrast to biogenic inorganic materials,[xxv] interfacing MOFs with gelatin was only rarely reported.[xxviii] In the present work, the thermo-reversible character of gelatin associated to a liquid-liquid phase separation process (i.e. coacervation)[xxix] was exploited to prepare a series of gelatin/UiO-66-X (X=H, CF$_3$, NH$_2$) and gelatin/MOF-801 composites that combine attractive features such as a high MOF loading (> 80 wt%), high porosity, an homogeneous MOF distribution and a tunable hydrophobic-hydrophilic balance. Note that the main advantage of using biomacromolecules such as gelatin is related to its chemical complexity, multifunctionality and polyelectrolyte nature to which no synthetic equivalent is available. This enabled the integration of hydrophilic as well as hydrophobic MOFs into the water-soluble gelatin.

Finally, these MOF-gelatin composites could be shaped in different forms (films or monoliths) on large scale and have shown a high performance for the selective capture of acetic acid (AA) under humid ambient conditions. The emission of AA is a major concern in cultural heritage (CH) for the preservation of cellulose based artefacts such as papers, books, photographic films etc…[xxx] More than 75 years of visual and audio memories are actually in serious danger due to the hydrolysis and oxidation of cellulose acetate into AA.[xxxi,xxxii] A viable solution to protect CH artefacts consists of using adsorbents such as activated carbons, zeolites, silica and pillared clays to efficiently capture AA.[xxxiii,xxxiv] However, AA raises additional challenges compared to other less hydrophilic molecules, due to its potential competitive adsorption with water under relative humidity (RH) above 30%. Zeolites such as NaY or NaX, are strongly hydrophilic which makes them readily saturated by water even at very low RH[xxxiv] thus considerably reducing their AA adsorption efficiency. On the contrary, activated carbons, usually more hydrophobic generally suffer from a low AA uptake capacity owing to their relatively poor affinity for AA. Therefore, the search of alternative and more efficient adsorbents that combine large AA adsorption capacity and high AA/water selectivity is still a great challenge for the CH conservation. Recently, some of us have recently shown that UiO-66(Zr) and UiO-66-(Zr)(CF$_3$)$_2$ present a good performance for the capture of AA in presence of water.[xxxv] In particular, UiO-66-(Zr)(CF$_3$)$_2$ is able to overpass the benchmark adsorbents (NaY zeolite and RB4 activated carbon) in terms of AA/H$_2$O selectivity thanks to its hydrophobic character, suitable pore size for adequate confinement and specific interactions owing to the grafted CF$_3$ functions.[xxxv] In the present article, we have shown that UiO-66-X/gelatin composites can be considered as a novel type of highly efficient adsorbents in CH preservation.

Experimental

Chemicals

All chemicals were commercially available and used without further purification. Commercial gelatin extracted from porcine skin (type A with a bloom of 175 g) corresponding to an average molecular weight of 40000 g mol^{-1} and an isoelectric point (I.E.P) of about 8 (according to the supplier) was purchased from Sigma-Aldrich. Other chemicals were purchased from Sigma-Aldrich or Merck.

Preparation of gelatin solutions.

Gelatin solutions (1-10 wt %, in aqueous solution) were prepared by swelling the gelatin granules in an aqueous solution for a minimum period of 3 h at a temperature of 5 °C. Gelatin was then dissolved at a temperature of 50 °C, using a magnetic stirrer for 30 min at 300 rpm.

Synthesis of MOF-gelatin hydrogel composites by coacervation.

In this approach, the MOFs were formed in-situ in the presence of a gelatin coacervate.

Step 1. To a 20 mL scintillation vial were added 71 µL of a 70% zirconium propoxide [Zr(OPr^n)$_4$] solution in 1-propanol (0.0519 g, 0.158 mmol), 7 mL of DMF, and 4 mL of acetic acid (4.196 g, 70 mmol). The solution was heated in an aluminium block on a hot plate at 130°C for 2 h during which a noticeable change in solution color from colorless to yellow was observed. Then the solution was cooled at RT.

Step 2. To 11 mL of the {Zr$_6$} oxo-cluster solution (0.158 mmol) obtained from step 1, 0.5 mmol of any one of the ligands (84 mg of 1,4 benzene dicarboxylic acid (bdc), 151 mg of bdc-(CF$_3$)$_2$, 90.5 mg of bdc-NH$_2$ and 58 mg of fumaric acid(FA)) was added. The mixture was stirred for 15 minutes until a homogeneous dispersion was obtained. Then, 2 mL of 10 wt% gelatin was added to this solution and stirred for 10 minutes followed by the addition of 2 mL of ethanol. Finally, the mixture was stirred at room temperature (RT) (20°C) for 24 h to obtain the hydrogel composites.

### Processing of the MOF-gelatin composite films and tablets

After macroscopic phase separation, the composite hydrogels were heated with their supernatant solution at 70 °C for 15 min and then 90 °C for 5 min before being poured without their supernatant solution into rectangular molds (length = 6 cm, width = 9 cm) thermalized at 70 °C. In order to avoid the formation of a brittle surface due to drying, which could not be reversibly reswollen, the molds are immediately capped in an almost hermetic manner. Using different molds, coatings and tablets were finally formed by cooling at RT for 15 min and then kept at 2 °C for 1 day. Prior to the adsorption experiments all materials were activated in high vacuum (10^{-6} mbar; HiCube 80, Pfeiffer Vacuum) for 4 hours at 150ºC.

Results and discussion.

Synthesis of UiO-66-X (X = H, NH$_2$, (CF$_3$)$_2$) and MOF-801 nanoparticles.

For the design of MOF/gelatin composites, we considered a series of microporous MOFs with the UiO-66 type framework. The idealized structure of UiO-66 can be described by the assembly of {Zr$_6$O$_4$(OH)$_4$} secondary building unit (SBU) with 12 ditopic 1,4 benzene dicarboxylate (1,4-bdc) linkers, resulting in a crystalline structure with face-centered cubic (fcu) topology (Fig. 1).$^{Erreur ! Source du renvoi introuvable.}$ We have also selected a series of isostructural analogues such as the UiO-66-X functionalized derivatives (X=NH$_2$, (CF$_3$)$_2$) that can be obtained by using bdc linker grafted with either -NH$_2$ or -CF$_3$ groups, [xxxv,xxxvi,xxxvii] as well as the fumaric acid (FA) analogue MOF-801.[xxxviii,xxxix,xl] This whole series of MOFs was synthesized through RT two-steps protocol previously reported by Farha *et al.*[xli] (See Supporting Information (SI) for details.). First, it implies the synthesis of the [Zr$_6$O$_4$(OH)$_4$(OAc)$_{12}$] (OAc = acetate) oxo clusters, which react in a second step with the organic linker (bdc-X (X=NH$_2$, (CF$_3$)$_2$) or FA). These materials were characterized by combining powder X-ray diffraction (PXRD), thermogravimetric analysis (TGA), FT-IR, N$_2$ porosimetry, scanning and transmission electron microscopy (SEM, TEM, HAADF-STEM and STEM-XEDS) (see SI for details). The PXRD pattern of these MOFs display the characteristic Bragg peaks of the UiO-66 type structure (Fig. S3). UiO-66 consists of spheroidal nanocrystals with an average particle diameter of 70 nm and a quite large distribution in diameter between 40 and 200 nm (Fig. S7 & S8). In contrast, UiO-66-X (X= NH$_2$, (CF$_3$)$_2$) and MOF-801 samples are made of nanocrystals whose diameter (~30 nm for UiO-66-NH$_2$ and MOF-801, ~15 nm for UiO-66-(CF$_3$)$_2$) are significantly lower than that UiO-66. (Fig. S10, S11, S13 & S14), in agreement with the presence of broad Bragg peaks on their PXRD patterns. This series of MOF was synthesized by using a high concentration of modulator (i.e. acetic acid, AA, 443 eq.) that not only affords control over the crystal size but also the density of defects.[xlii,xliii,xliv] Moreover, this addition of modulator can strongly affect the porosity, the hydrophilic-hydrophobic balance of the MOFs and their adsorption or catalytic properties as previously reported.[xlv,xlvi,xlvii,xlviii,xlix,l] Defects arise when an organic linker (linker defects) or an entire zirconium cluster and its 12 associated linkers (cluster defects) are missing, resulting in the formation of open coordination sites on SBUs. As previously reported, charge-compensation of these sites is mainly achieved through the capping of these uncoordinated Zr sites with either OH/H$_2$O or modulator (here acetate).[xli-xlvii] The composition and amount of structural defects of this series of MOF was determined by combining TGA, ^{1}H &^{13}C MAS NMR spectroscopy (see SI for details) as previously reported for defective UiO-66.[xlv-xlvii] Table 1 indicates the chemical composition of MOFs as well as their defect level which can be defined as the average number of missing linkers per Zr$_6$ node. These MOF shows a quite high amount of defects since the connectivity of the {Zr$_6$} clusters ranges between 10 (UiO-66 and UiO-66-NH$_2$), 9 (MOF-801) and 8 (UiO-66(CF$_3$)$_2$) while this connectivity is 12 for an ideal defect-free UiO-66. UiO-66 and UiO-66-NH$_2$ presents an amount of defects which is comparable to that previously reported for these MOFs prepared with similar amount of modulator.[xli,xlviii,li] Neither TGA nor ^{1}H &^{13}C MAS NMR are able to differentiate between missing-linker and missing-linker defects. However, correlated missing-cluster defects can result in a defected reo phase that exhibits one broad peak at low angle, typically 3-8° 2θ range.[xlv] Such broad peak was not observed in the PXRD pattern of these MOFs. Therefore, if these MOFs contain missing clusters defects, their density is presumably quite low and/or they are randomly distributed in the MOF frameworks. These MOFs were also characterized by N$_2$ adsorption/desorption isotherms (see Fig. 2) at 77 K. UiO-66 presents a

type-I isotherm which is consistent with the microporous structure of this MOF (cages of 8 and 11 Å in diameter). In contrast, the isotherms of the other MOFs are combinations of type I and type IV isotherm, indicating that these MOF contain both micropores and mesopores. The hysteresis between the adsorption and desorption branches are characteristic of mesopores. As indicated by pore size distribution (PSD) derived from the Barrett-Joyner-Halenda (BJH) pore-size model (see Fig. S6), UiO-66-X (X=NH$_2$, (CF$_3$)$_2$) exhibit a distribution of large mesopores of approximately 3.5-12 nm in diameter that correspond presumably to interparticle voids as a result of the strong aggregation of MOF nanoparticles (NPs). Similarly MOF-801 contain also intercrystal mesopores of about 20 nm in diameter but also small mesopores of about 2 nm that might correspond to the presence of missing cluster defects. [li,lii] In contrast, the presence of mesopores resulting from missing cluster defects was not evidenced for UiO-66-X (X=H, NH$_2$, (CF$_3$)$_2$), meaning that these MOF contain presumably mainly missing linker defects
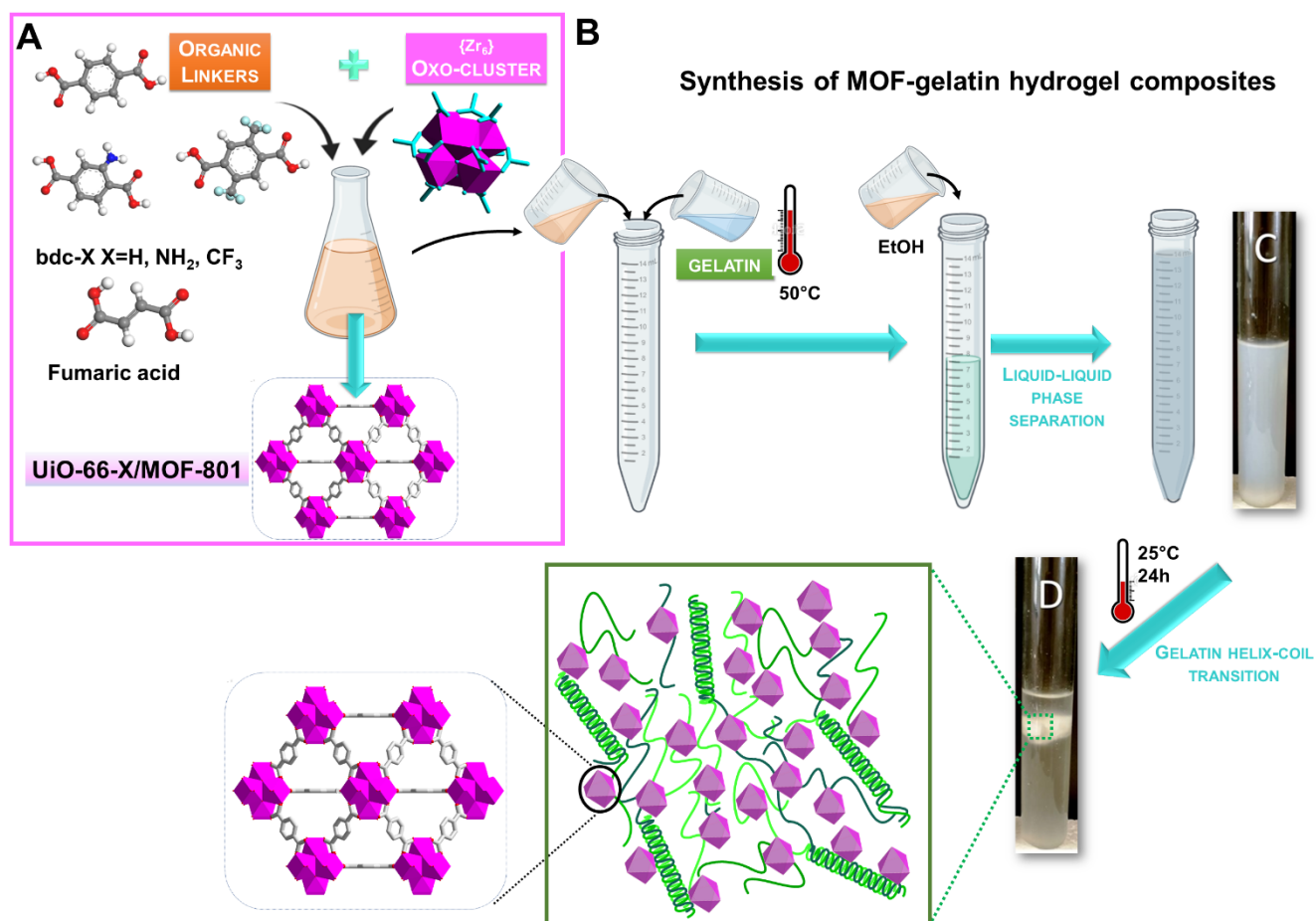

Fig. 1. Schematic drawing of A) the room-temperature synthesis of UiO-66-X (X =H, NH$_2$, (CF$_3$)$_2$) and MOF-801, B) the synthesis approach of the UiO-66-X (X =H, NH$_2$, (CF$_3$)$_2$)/gelatin and MOF-801/gelatin composites. C) and D) are photographs of UiO-66/gelatin hydrogels obtained just after the addition of ethanol (C) and after ageing at RT for 24h (D). Zr polyhedral, carbon, oxygen, nitrogen, fluoride, hydrogen are in pink, grey, red, blue, green and white respectively

Synthesis of MOFs/gelatin hydrogel composites through coacervation.

Gelatin/MOF composites were then prepared through the blending of these preformed MOF particles into physical gel of gelatins. Indeed, gelatin is soluble in water above the temperature of gelification (close to 27 °C for a mammalian gelatin) but forms reversible physical gels below this temperature.[liii] The UiO-66-gelatin hydrogels were prepared by mixing UiO-66 NPs and gelatin aqueous solutions at 40°C (see SI for details) and pH 3, followed by cooling to 4°C to induce the physical gelation of gelatin. Unfortunately, these hydrogels present a very low amount of UiO-66 whatever the initial amount of gelatin and MOF, as revealed by the very low intensity of the characteristic PXRD peaks and FTIR vibrations of UiO-66 (Fig. S2). Moreover, the UiO-66 content of hybrid hydrogels remains low even though MOF and gelatin were mixed in pH conditions (pH 7) for which they exhibit opposite electrostatic charge (the point of zero charge of UiO-66 NPs is close to 6 (Table S1) while the isoelectric point of gelatin is equal to 8).[liiii]

In order to enhance the MOF rate in hydrogels, we took profit of the coacervation process which is widely used as an efficient formulation tool for the microencapsulation of drugs and cosmetics.[xxix,liv,lv] This is a liquid-liquid phase separation process that takes place by adding a "non-solvent" to the polymer solution. Herein, the phase separation of gelatin was induced by adding ethanol (non-solvent) to an aqueous solution of gelatin.[lvi] Gelatin is a polyampholyte, containing both positively and negatively charged amino acid residues in the polymer backbone. In the presence of the non-solvent, sequential intermolecular charge neutralization of gelatin molecules occurs leading to the aggregation of gelatin molecules in the aqueous phase.[lvi] This phenomenon gives thus rise to the formation of a gelatin-rich and gelatin-lean solution phase. This coacervation process is thus particularly useful to increase the gelatin concentration in hydrogels.[lvii,lviii] As previously reported, the gelatin concentration of gelatin coacervate can reach a value of 45 wt% while it does not exceed 15 wt% for hydrogels prepared through simple gelatin dissolution (physical gelation).[lvii,lviii] In this study, simple coacervation process of gelatin was coupled with *in situ* formation of UiO-66(Zr) NPs (see Fig. 1) The two-steps synthesis of UiO-66(Zr) NPs at RT as previously used for the synthesis of pure MOF was thus conducted by reacting the $\{Zr_6\}$ oxo-cluster and the bdc linker with gelatin aqueous solution (10 wt%, pH 7) and non-solvent ethanol (Fig. 1C, see SI for more details). Keeping this dispersion stirring at RT for 24 hours leads to a phase separation between a white visco-elastic hydrogel (Fig. 1D) and an ethanol solution. To the best of our knowledge this is the first time that MOF based hydrogels are synthesized from a coacervation process. The PXRD pattern of UiO-66/gelatin composite (UiO-66/G) displays sharp and intense Bragg peaks of UiO-66 in agreement with the formation of highly crystalline UiO-66(Zr) (Fig. 2b). According to TGA and inductively coupled plasma atomic emission spectroscopy (ICP-AES), the composite contains a large UiO-66 amount of about ~88 wt%. Similar syntheses of UiO-66-X/G (X = NH$_2$, (CF$_3$)$_2$) and MOF-801/G composites were performed by keeping constant all the physico-chemical parameters of the preparation of hydrogel composites (concentrations of precursors, pH, duration, etc…) in order to compare the affinity of gelatin with different functionalized MOFs. The PXRD patterns of the composite hydrogels present the characteristic Bragg peaks of the parental MOFs, in agreement with the formation of these MOFs under the coacervation conditions (Fig. 2). However, while the PXRD pattern of UiO-66/G displays sharp and intense Bragg peaks, the peaks of the other composites are much broader. This suggests that the MOF particles in UiO-66-X/G and MOF-801/G composites are smaller than that of UiO-66/G (Fig. 2 and S3) as shown by SEM and TEM (vide supra). According to TGA and ICP-AES, these bionanocomposites present also a high MOF loading (> 50 wt%) (see Table 1). These MOF/G hydrogel composites consist presumably of MOF particles distributed in physically cross-linked gelatin gels that can be described as an entangled assembly of rigid triple helices connected by flexible links. Indeed, the sol-gel transition of gelatin and thus the partial renaturation of collagen triple helices is likely to take place during the coacervation process by decreasing the temperature.[xxv,liii] The presence and relative quantification of gelatin triple helices in the composites was thus determined by differential scanning calorimetry (DSC). For the whole series, the DSC thermograms (Fig. S16a) are characterized by a broad endothermic peak corresponding to two superimposed phenomena related to the water vaporization and the melting of gelatin triple helices. By assuming a heat of water vaporization of 100 J.g^{-1}, it was possible to extract the heat of gelatin triple helices melting that qualitatively reflects the amount of gelatin triple helices.[lviii,lix] As shown in Fig. S16b, the amount of gelatin triple helices linearly increases with the amount of gelatin and this tendency is fully consistent with that observed for previously reported gelatin hydrogels.[lviii] Since the gelatin concentration varies from 9, 12, 30 and 49 wt% for UiO-66(CF$_3$)$_2$/G, UiO-66/G, UiO-66(NH$_2$)/G and MOF-801/G respectively, the gelatin triple helices content is significantly higher for UiO-66 (NH$_2$)/G and MOF-801/G than that of UiO-66/G and UiO-66(CF$_3$)$_2$/G. The acetate/organic linker molar ratio of the MOFs in the MOF/G hydrogels evaluated by ^{1}H/^{13}C solid state NMR (Fig. S22-S33) was compared to that of pure MOFs. Prior to NMR acquisition, MOF/G hydrogels were thoroughly washed in water to partially remove gelatin. However, the quantification of FA and acetate in the MOF-801/G sample was not possible due to the remaining large amount of gelatin. For the other MOF/G hydrogels, the acetate/organic linker molar ratio and thus the amount of defects in the MOF/G composites is comparable (UiO-66/G) or significantly lower (UiO-66-X/G (X = NH$_2$, (CF$_3$)$_2$) than that of the parental MOFs. These results show that gelatin is prone to affect the creation of defects in the MOF framework. As shown by N$_2$ sorption at 77 K, the BET area of UiO-66/G composite decreases by ~30% to 1083 m^2.g^{-1} in comparison to the pure UiO-66 (1560 m^2.g^{-1}). To exclude the weight percentage of the non-porous gelatin (i.e. 12 wt%), the adsorption isotherm of UiO-66/G was normalized to the weight of the MOF only, giving a normalized BET area close to ~1230 m^2 g^{-1}. This indicates that the UiO-66/G composite is highly porous and still retains 79 % of the BET area of the parent MOF. Similarly to UiO-66/G, the normalized BET area of UiO-66-X/G (X = NH$_2$, (CF$_3$)$_2$) and MOF-801/G calculated by considering the MOF content of these composites show that these materials kept more than 68% of the BET area of the pristine MOF (see Table 1). Accordingly, the normalized micropore volumes of MOF/G composites are similar to that of the parental MOFs, indicating that the micropores of the MOFs are thus not infiltrated by gelatin. In contrast, one can observe a strong decrease of the mesopore volume of UiO-66-X/G (X = NH$_2$, (CF$_3$)$_2$) and MOF-801/G in comparison to the parental MOFs. The normalized mesopore volume decreased of about 57%, 52 % and 15 % for UiO-66(CF$_3$)$_2$/G, UiO-66(NH$_2$)/G and MOF-801/G. This observation can be explained by a partial penetration of gelatin chains and triple helices in MOF

interparticle voids since such mesopores are accessible to the gelatin triple helices with diameter and length of 1.5 nm and 300 nm respectively.[lx] The high accessibility of micropores and partial mesopores clogging by gelatin in MOF/G composites is confirmed by BJH-PSD analysis (see Fig. S6).The microstructure of composites as well as the morphology of entrapped MOF particles were investigated by combing SEM & TEM experiments. First, prior to the SEM and HAADF-STEM observations, the MOF/G were washed in water in order to remove a large amount of gelatin. The SEM and TEM images (see Fig. 3e and Fig. S9a-b) clearly show that UiO-66/G consists of highly monodisperse and well-defined octahedral crystals with a diameter of 350 nm. In contrast, UiO-66-X (X = NH$_2$, (CF$_3$)$_2$) and MOF-801/G composites are made of spheroidal and much smaller MOF NPs with diameter of about 30 nm for UiO-66-NH$_2$/G and MOF-801/G and 15 nm for UiO-66(CF$_3$)$_2$/G, as shown by HAADF-STEM images (see Fig. 4 and S15). Remarkably, the MOF NPs formed within gelatin present an homogeneous morphology and a low size distribution. The spatial distribution of MOF particles in the as-prepared MOF/G hydrogels was also characterized by combining TEM and SEM of fractured samples. The top surface and cross-section SEM images of UiO-66-X (X = NH$_2$, (CF$_3$)$_2$) and MOF-801/G composites show an excellent dispersion of MOF NPs in the gelatin matrix with the absence of any significant aggregation and phase separation (see Fig. 3, 4 and S15). Remarkably, UiO-66-X (X = NH$_2$, (CF$_3$)$_2$) and MOF-801/G exhibit an organized lamellar texture as revealed by the presence of oriented steps (Fig. 3). This gelatin organization was typically observed for pure physical gelatin hydrogels as previously shown.[lvii] The distribution of MOF particles in the UiO-66/G sample was difficult to observe by classical SEM observations due to the larger diameter of MOF particles. We thus relied on the TEM observation of ultramicrotomed hydrogel samples with a fixed thickness (80 nm). This allows MOF particles to be clearly visualized in the entire volume of the composite. It is known that MOF particles are prone to aggregate upon drying and this phenomenon is even more pronounced as the MOF particle size increases and the MOF/polymer interactions are weak. However, according to the TEM images of ultrathin slices of UiO-66/G (Fig. 3a and S9c-d), MOF particles are remarkably well distributed in the gelatin matrix with the absence of phase separation and particle aggregation despite the high diameter of UiO-66 particles. These observations reveal a high compatibility between gelatin and this series of functionalized MOFs. Note that the highest MOF content of about 91 wt% is obtained with the hydrophobic UiO-66(CF$_3$)$_2$ MOF while gelatin is a hydrophilic and water soluble biopolymer. In contrast, despite the hydrophilic character of MOF-801, the corresponding MOF-801/G hydrogel contains the lowest MOF amount (~51 wt%).
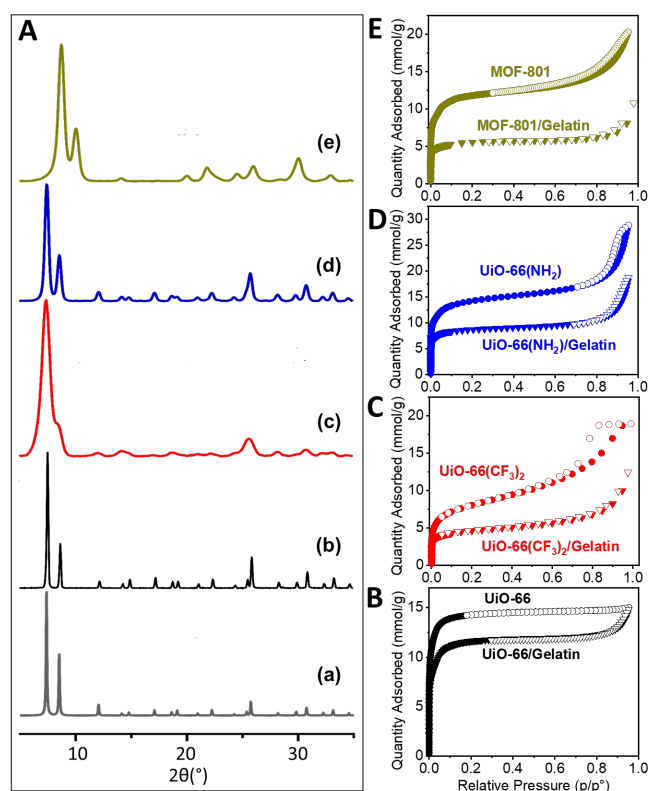
Fig. 2. A) a) calculated PXRD pattern of UiO-66, Experimental PXRD pattern of b) UiO-66/G, c) UiO-66(CF$_3$)$_2$/G, d) UiO-66(NH$_2$)/G, e) MOF-801/G, B-E) N$_2$ adsorption-desorption isotherms (adsorption, filled symbols; desorption, empty symbols) at 77 K (P° = 1 atm) of B) UiO-66 & UiO-66-G, C)UiO-66(CF$_3$)$_2$ & UiO-66(CF$_3$)$_2$/G, D) UiO-66(NH$_2$) & UiO-66(NH$_2$)/G and E) MOF-801 &MOF-801/G

Hybrid material	AcO/L[a]	Molecular formula of MOF[b,c]	Defect level (%)[d]	MOF content (wt%)[b]	Connectivity of $\{Zr_6\}$ oxo cluster	S_{BET} $(m^2 \cdot g^{-1})$	Pore volume $(cm^3\ g^{-1})$
UiO-66(Zr)	0.20	$Zr_6O_{5.2}(OH)_{2.8}(bdc)_{4.9}(AcO)_{1.0}$	18.3		10	1560	0.56
UiO-66(Zr)/G	0.20	-		88	-	1083	0.46
UiO-66(Zr)-NH$_2$	0.45	$Zr_6O_4(OH)_4(bdc\text{-}NH_2)_{5.0}(AcO)_{2.0}$	16.6		10	1243	0.48
UiO-66(Zr)-NH$_2$/G	0.30	-		70	-	790	0.3
UiO-66(Zr)(CF$_3$)$_2$	0.70	$Zr_6O_{4.6}(OH)_{3.4}(bdc\text{-}(CF_3)_2)_{4.2}(AcO)_{3.0}$	30		8.4	649	0.27
UiO-66(Zr)(CF$_3$)$_2$/G	0.43	-		91	-	397	0.16
MOF-801(Zr)	0.62	$Zr_6O_{4.3}(OH)_{3.7}(FA)_{4.5}(AcO)_{2.7}$	25		9	1020	0.43
MOF-801(Zr)/G		-		51	-	572	0.23

[a]determined by ^1H & ^{13}C MAS NMR, L= organic linker (bdc, bdc-NH$_2$, bdc-(CF$_3$)$_2$, FA), [b]determined by combining TGA and ^1H & ^{13}C MAS NMR, [c] bdc : benzene dicarboxylic acid, FA: fumaric acid, AcO: acetate, [d]the defect level is the average number missing linkers per Zr$_6$ node which is the average number of defects divided by the ideal number of linkers per formula unit (6 for UiO-66).
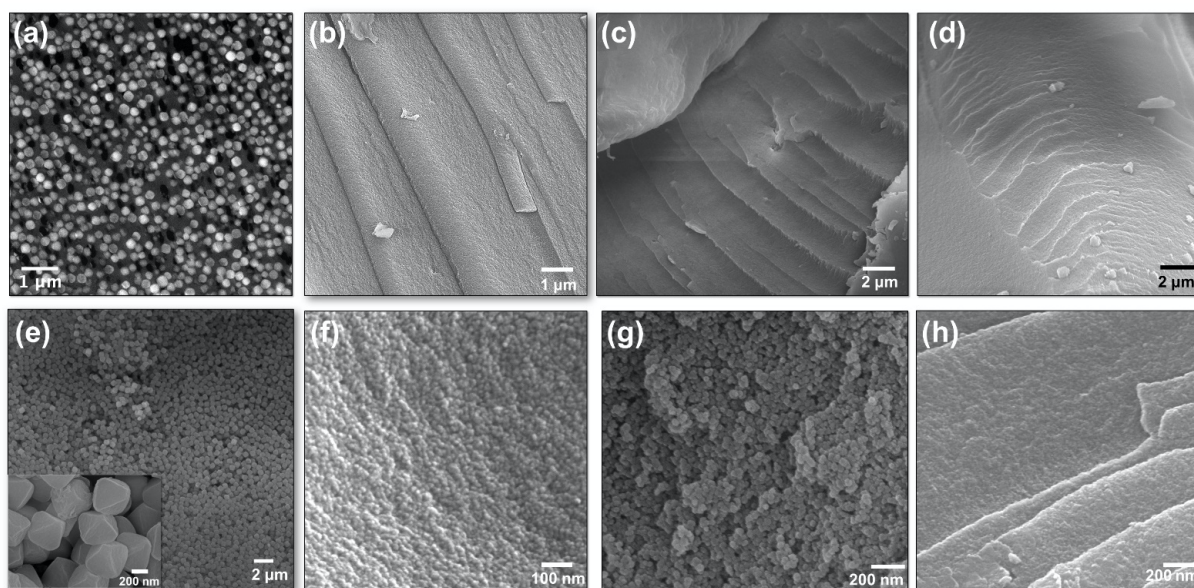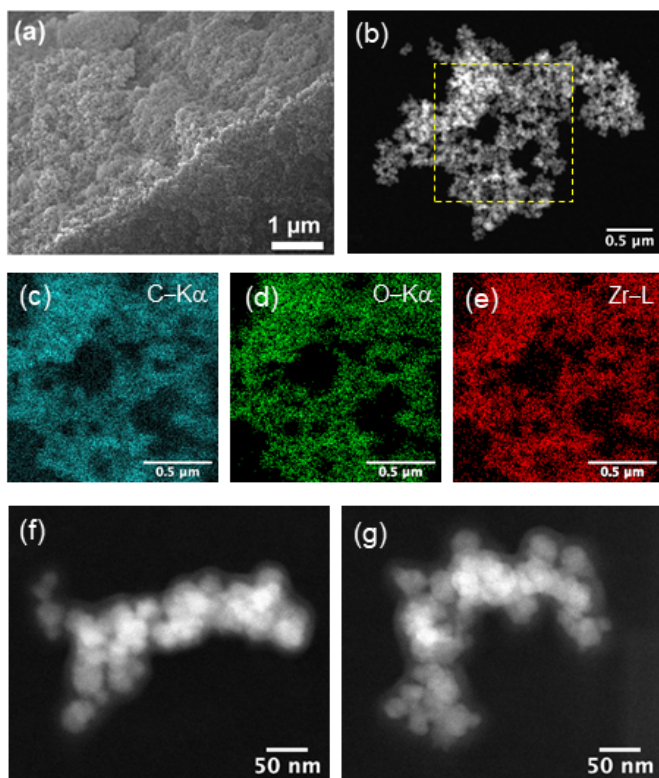

Fig. 3. (a) TEM image of 100 nm ultramicrotomed slice of UiO-66/G hydrogel, (e) SEM images of UiO-66/G hydrogel after washings in water, (b, f) SEM images of UiO-66(CF$_3$)$_2$/G, (c, g) SEM images of UiO-66(NH$_2$)/G, (d, h) SEM images of MOF-801/G

Fig. 4. (a) cross-section SEM image of UiO-66(NH$_2$)/G composite, (b,f,g) HAADF-STEM images UiO-66(NH$_2$)/G composite and (c-e) STEM-XEDS elemental mapping of the area related to the yellow dashed square in (b). For images (b-g), the composite was washed in water to remove partially gelatin.

This indicates that the hydrophilic-hydrophobic balance of the MOF is not the driving force for the incorporation of MOF with gelatin. The good compatibility of gelatin with this series of UiO-66-X/MOF-801 materials is certainly related to the high chemical functionality of the gelatin backbone that consists of about 20 different amino acid residues with charged, polar and coordinative groups able to interact with the MOF NPs as discussed below.

Characterization of the interfacial properties of MOF/gelatin composites: FT-IR/solid state NMR spectroscopies and molecular modelling.

To unravel the origin of the good compatibility between MOFs and gelatin, the bionanocomposites were characterized by combining FT-IR, multinuclear solid state NMR (^{1}H, ^{13}C, ^{19}F, ^{15}N) spectroscopies and the gelatin/MOF surface interactions were computationally explored using Density Functional Theory (DFT) calculations. The FT-IR spectra of composites display the characteristic vibration bands of the parental MOFs and gelatin, with only a slight shift of their position as a result of weak interactions between MOFs and the amino acid residues of gelatin (see Fig. S4 and Table S3). Similarly, the ^{1}H MAS and ^{13}C{^{1}H} CP MAS spectra (Fig. S17 & S19) of MOF/G composites display the characteristic signals of the parental MOF and gelatin with similar ^{1}H and ^{13}C chemical shifts than those of the pure components, thereby showing the absence of any covalent cross-linking between gelatin and the MOFs. In addition, ^{19}F MAS and ^{15}N(^{1}H) CP MAS NMR spectra of UiO-66(CF$_3$)$_2$/G and UiO-66(NH$_2$)/G respectively (Fig. S20 & S21) indicate also that the functional groups (CF$_3$ and NH$_2$) of the organic linkers of UiO-66-X (X = NH$_2$, (CF$_3$)$_2$) do not strongly interact with gelatin. The MOF/G interfacial interactions were finally assessed by molecular modelling considering that gelatin presents a repetitive amino acid sequence (Gly-Xaa-Yaa)n. In a mammalian gelatin, every third amino acid is thus glycine (Gly) while Xaa is often (2S)-proline and Yaa is mostly (2S,4R)-4-hydroxyproline (Hyp) or alanine (Ala).[xxv,lx] Therefore, cluster models that mimic the external surface of UiO-66 and UiO-66(CF$_3$)$_2$ were put into contact with either Gly-Pro or Gly-Ala dipeptides sequence (Fig. S34). The termination scheme of these cluster models cleaved from the periodic DFT-optimized bulk structures involves the capping of the Zr atoms by OH group.[lxi] Several initial configurations for Gly-Ala and Gly-Pro in interaction with both clusters were considered and further geometry optimized. The most stable configurations are presented in Fig. 5. Fig. 5c shows that the amino and carboxyl functions of Gly-Ala interact strongly via their hydrogen and oxygen atoms, respectively with the terminal hydroxyl groups of UiO-66(Zr) forming hydrogen bonds with associated short separating distances ranging from1.5 and 1.7 Å. The oxygen atom of the peptide function equally forms a hydrogen bond with the terminal hydroxyl groups of UiO-66(Zr). In the case of the UiO-66(Zr)(CF$_3$)$_2$, the presence of the grafted functions to

the organic linkers substantially changes the preferential orientation of the Gly-Ala motif as compared to the scenario encountered for UiO-66(Zr) and favors the formation of a hydrogen bond between the amino function of the molecule and the $-CF_3$ group (Fig. 5e). Notably, this additional dipeptide/MOF surface interaction drives a proton transfer from the terminal NH_3^+ to the neighbor terminal hydroxyl groups of the MOF as illustrated in Fig. 5e. The resulting interaction energy between Gly-Ala and UiO-66(Zr)-$(CF_3)_2$ (-138.6 kcal mol^{-1}) is therefore substantially higher compared to the pristine UiO-66(Zr) (-93.9 kcal mol^{-1}). Remarkably, Gly-Pro behaves similarly as illustrated in Fig. 5d-f. One can observe that this molecule adopts preferential conformations in such a way to form strong hydrogen bonds between its terminal carboxyl, amino and peptide functions with the MOF hydroxyl groups for both UiO-66(Zr) while the additional interaction with the $-CF_3$ group still favors the proton migration from NH_3^+ to the OH terminal group of UiO-66(Zr)-$(CF_3)_2$. This results to a significantly higher interaction energy for UiO-66(Zr)-$(CF_3)_2$ (-112.5 kcal mol^{-1}) as compared to UiO-66(Zr) (-85.4 kcal mol^{-1}). This set of prediction supports stronger overall interactions between gelatin and the functionalized UiO-66(Zr)-$(CF_3)_2$. This high compatibility between MOFs and gelatin leads to the enrichment of MOF in the gelatin-rich aqueous phase during the coacervation process as observed experimentally. Gelatin, being a polyampholyte could thus act as a MOF NP stabilizer and buffer.
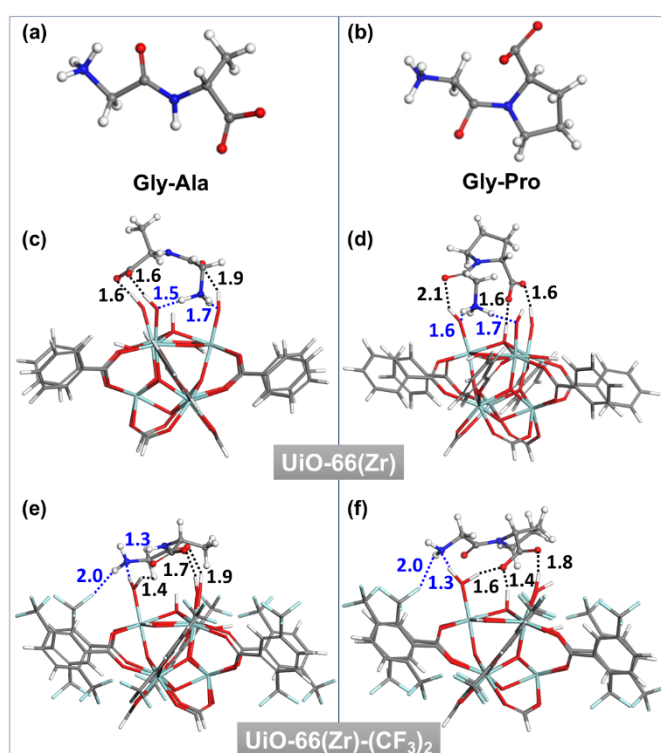

Fig. 5. (a,b) Molecular structure of Gly-Ala and Gly-Pro dipeptides, (c-e) Illustration of the main interactions between (c) UiO-66(Zr) and Gly-Ala, (d) UiO-66(Zr) and Gly-Pro, (e) UiO-66(Zr)-$(CF_3)_2$ and Gly-Ala, and (f) UiO-66(Zr)-$(CF_3)_2$ and Gly-Pro. Color code: C, gray, N, blue, O, red, H, white, F, green

### Influence of gelatin on the nucleation and growth of MOF.

As a further stage, to investigate the impact of gelatin on the nucleation and growth of MOF, the diameter and morphology of MOF particles in MOF/G composites was compared to that of pure MOFs. Note that the presence of gelatin induces the formation of UiO-66 with much larger particle size (average diameter 350 nm versus 70 nm for the pure UiO-66) and a narrow diameter distribution. In contrast, UiO-66-X (X = NH_2, $(CF_3)_2$) and MOF-801/G samples are made of nanocrystals whose morphology and diameter (~30 nm for UiO-66-NH_2 and MOF-801, ~15 nm for UiO-66-$(CF_3)_2$) are comparable to those present in pure MOF (Fig. 3-4, S7-S15). These result show that gelatin acts as a molecular modulator for the formation of UiO-66 while this biopolymer exerts no kinetic control of the crystallization of UiO-66-X (X = NH_2, $(CF_3)_2$) and MOF-801. Polymers and biopolymers have already sparked a great interest as modulators for morphogenesis of MOFs.[Erreur ! Signet non défini.],[lxii] In particular, a concentration-dependent influence of gelatin on the nucleation/growth of HKUST-1 was previously observed.[xxviii] In the present work, MOF NPs are synthesized by using an excess of AA which served as a complexing ligand for the formation of $[Zr_6O_4(OH)_4(OAc)_{12}]$ oxo cluster and as a modulator for controlling the crystal growth of MOF. As previously reported, the MOF nanocrystal size results from a subtle interplay between different equilibria such as linker deprotonation,

linker complexation, modulator deprotonation and termination.[lxiii,lxiv] It was clearly shown that the presence of monocarboxylic acid such as AA can increase or reduce the crystal size of UiO-type MOFs depending on whether these molecules can limit the organic linker deprotonation or act as surface capping ligand.[lxiii,lxiv,]**Erreur ! Source du renvoi introuvable.** An acid modulator with a significant amount has the effect of limiting the deprotonation of the ligand upon decreasing pH and can also compete with the organic linker for the metal coordination, thereby slowing down the metal-ligand complexation and leading to large particle sizes.[lxiii,lxiv] The role of gelatin as a modulator of UiO-66 compares thus very well with that of monocarboxylic acids. Note that the role of L-proline as an efficient modulator was shown for the formation of Zr and Hf MOFs.[lxv] In the case of gelatin, this is certainly due to the presence of the carboxylate side chains of the glutamate (Glu) and aspartate (Asp) residues.[xxviii] Note that AA as well as the carboxylate side chains of the Asp and Glu residues exhibit a similar pKa value than that of the organic linker of UiO-66 (pKa(AA) = 4.20 and pKa (1,4-bdc) = 4.82 and 3.5, pKa (Asp) = 3.71 pKa (Glu) = 4.15) and this may explain the high level of coordinative competition between modulators (AA and gelatin) and the organic linker. Note that these literature pKa values are measured in aqueous solution while MOF/G composites were synthesized in a mixture of aqueous/organic solvents. But they can qualitatively explain the observed trends. In comparison, UiO-66-NH_2/MOF-801 and UiO-66-$(CF_3)_2$ NPs in the hydrogel composites are 11 and 23 times smaller than that of UiO-66 NPs which means that the addition of gelatin interferes to a less extent with linker deprotonation. The strong acidity of $(CF_3)_2$-bdc linker (pKa = 1.1) may induce a fast nucleation process, leading to very small MOF nanocrystals. Therefore, gelatin is not able to impede the deprotonation of the $(CF_3)_2$-bdc linker even at high concentration. In summary, gelatin exerts mainly a kinetics control on the formation of the non-functionalized UiO-66 nanocrystals. The absence of any covalent cross-linking between these UiO-66 type MOFs and gelatin despite the presence of free carboxylate functions on the gelatin backbone is certainly due to the strong metal-bdc bond. This result is fully consistent with the absence of any post-synthetic ligand exchange previously observed by adding poly(amic acid) to UiO-66.[lxvi].

Processing of MOF/gelatin composites as adsorbents for the capture of acetic acid under humid ambient conditions.

In the final step, MOF/G composites were evaluated for the selective capture of AA under ambient humid conditions. For their practical use as AA adsorbents, the MOF/gelatin hydrogels were processed in different forms including thick coatings and tablets (see Fig. 6A) by taking advantage of the temperature-dependent sol-gel transition of gelatin (see SI for details). It is noteworthy that these shaped UiO-66/G composites could be used in real conditions and thus inserted in archive boxes of photographic films. To assess the performance of MOF/G composites for the capture of AA under real conditions, experiments were conducted by using an environmental chamber in the presence of water (Fig. 6B), that is, 40% RH typically present in museums. Minor amounts of AA were injected in the closed chamber (corresponding to 362 µg dm^{-3}) with controlled RH, allowing the measurement of comparative profiles of AA removal by the MOFs (100 µg dm^{-3} is equivalent to 40 ppm in volume). There is an initial increase of the AA concentration in the chamber due to the evaporation and diffusion of AA molecules to the sensor followed by a decrease due to the adsorption of AA by the adsorbents. In their absence, a fast increase is observed and an AA concentration as high as 200 µg dm^{-3} is maintained during 2h (see Fig.S35). First the AA co-adsorption properties of pure UiO-66-X (X = H, NH_2, $(CF_3)_2$) NPs were evaluated in the chamber. MOF-801 presents a poor AA/water adsorption selectivity in line with its very high affinity for water. The MOF-801/G composite was thus not considered as an AA adsorbent. As shown in Fig. 6B-b, the UiO-66-X (X = H, NH_2, $(CF_3)_2$) materials show very good AA adsorption capacity under humid conditions, in agreement with results previously reported.[xxxv] Then, the performance of UiO-66-X (X = H, NH_2, $(CF_3)_2$)/G composites for the selective capture of AA under humidity was tested in comparison to the corresponding pure MOFs, pure gelatin coacervates as well as the benchmark Na-Y zeolites (Fig. 6B). This series of UiO-66-X/G led to very interesting results outperforming the benchmark NaY adsorbents by decreasing the AA concentration down to 24.9, 30.2 and 22.4 µg dm^{-3} for UiO-66/G, UiO-66(NH_2)/G, and UiO-66(CF_3)$_2$/G respectively after 2 h of exposure (Fig. 6B). It is interesting to note that the pure gelatin coacervate sorbs AA but with considerably less efficiency (57.3 µg dm^{-3} after 2 hours). The best material was found to be UiO-66-$(CF_3)_2$/G for which the fastest decrease was observed, reaching 22.4 µg dm^{-3} after 2 h. The high AA/water adsorption selectivity of this composite can be mainly imparted by the parental MOF which shows a comparable profile for the AA removal (Fig. 6B). As shown by the AA adsorption isotherm (Fig. S36), UiO-66-$(CF_3)_2$ presents a very good AA adsorption capacity. Compared to UiO-66, UiO-66-$(CF_3)_2$ presents a higher affinity to AA due to the presence of hydrogen bonds between the MOF framework and AA (CH_3-C<u>O</u>OH...μ_3(O<u>H</u>) and CH_3-COO<u>H</u>...C<u>F</u>$_3$) and its higher hydrophobicity as previously shown by molecular modelling.[xxxv] Note that the AA adsorption of pure gelatin and MOF/G composites measured by gravimetric isotherms is almost negligible (Fig. S36) and this may be due to their dehydration induced by the activation at 150 °C under vacuum prior to the isotherm acquisition. In those conditions, these hydrogels turn to glassy and non-porous materials in which the adsorption and diffusion of AA molecules is strongly limited. Therefore, the evaluation of the performance of adsorbents is more relevant by using the environmental chamber that fairly

reproduces the conditions of the application (RH between 40 and 60%). Finally, a series of hydrogels labelled as p-UiO-66-X/G were also prepared by using preformed UiO-66-X NPs (see SI for details) and then tested in similar conditions for the AA capture in humid conditions. However, their AA adsorption efficiency is lower in comparison to the first set of UiO-66-X/G hydrogels (see Fig. S37). This clearly indicates that the synthetic approach integrating the coacervation process and the *in-situ* formation of MOFs can lead to UiO-66-X/G adsorbents with excellent microstructural and textural properties for the selective capture of AA. Finally, the potential use of these composites for removing organic dyes from contaminated water was also evaluated. Shaped UiO-66 (X= H, CF$_3$)/G composites were thus immersed in an aqueous solution of 0.5 mM Reichardt's dye. After soaking for 15 min, the solution became colorless while the UiO-66/G composites became purple. The efficiency of UiO-66/G for the dye adsorption was confirmed by recording UV-vis spectra of the supernatant solutions (Fig. S38).
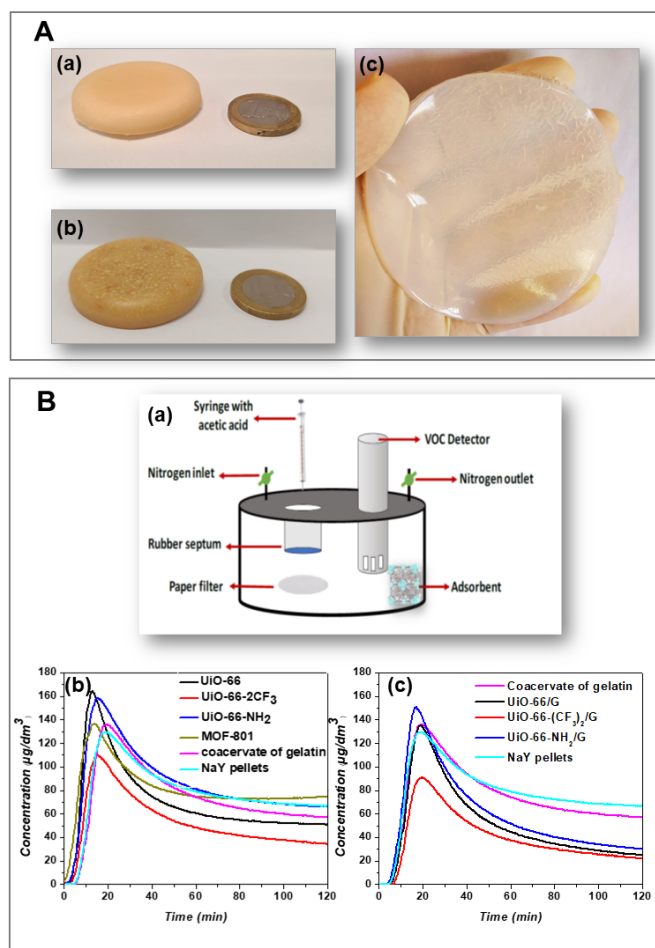
Fig. 6. A) photographs of shaped MOF/G composites : tablet of a) UiO-66/G, and b) UiO-66(CF$_3$)$_2$/G, c) coating of UiO-66/G; B) a) set-up of the environmental chamber used for the AA/H$_2$O co-adsorption studies b,c) AA concentration profiles inside a closed chamber after the injection of 1 μL of AA, at 25°C and 40% RH in the presence of 50 mg of different adsorbents including (b) MOFs and (c) UiO-66-X/G (X=H, NH$_2$,(CF$_3$)$_2$) composites. These AA concentration profiles are compared to that obtained with pure gelatin coacervate or NaY pellets

Conclusions

In summary, we report here a new and versatile approach for the synthesis at RT of green and eco-compatible hydrogel composites combining gelatin and Zr(IV) MOFs. This approach benefits from the thermo-reversible properties of gelatin and its phase separation by coacervation associated to the RT in-situ formation of UiO-66 type MOFs. This strategy was successfully applied to a series of Zr(IV) dicarboxylate MOFs (UiO-66 type MOFs and MOF-801) differing by their hydrophobic-hydrophilic balance and the functionalization of the organic linker. This enabled the production of hydrogel composites with interesting features such a high MOF content (> 50 wt%), a high porosity and an homogeneous MOF NPs distribution. This arises from an excellent compatibility between gelatin and MOF NPs as evidenced by a combination of advanced characterization techniques and molecular modelling. Such

composites could be shaped at the gram scale in different forms such as coatings and thick tablets. Finally, these shaped composites have shown high performance for the selective capture of AA under humid conditions. This paves the way for the use of these composites as adsorbents in CH preservation. Interestingly, our synthetic approach could be extended to other complex fluids whose combination with MOFs may lead to a wide range of MOFs based composites with a hierarchical porous structure.

Author Contributions

SB performed the synthesis and characterization of the MOFs and MOF-gelatin composites under the supervision of NS. MH characterized the MOF and MOF-gelatin composites by solid state NMR. CF and AAM performed the AA/water co-adsorption experiments under the supervision of MLP. CVS performed the molecular modelling under the supervision of GM. AS and CL characterized the MOF-gelatin composites by SEM. HZ characterized the MOFs and MOF-gelatin composites by N_2 porosimetry. FC performed DSC experiments on MOF-gelatin composites. NM performed TEM, HAADF-STEM and STEM-XEDS on MOFs and MOF-gelatin composites. NS wrote the article with the contribution and help of all authors.

Conflicts of interest

There are no conflicts to declare.

Acknowledgements

Notes and references

1 [i]
2 [ii]
3 [iii]
4 [iv]
5 [v]
6 [vi] Pierre D'Ans, Emilie Courbon, Anastasia Permyakova, Farid Nouar, Corine Simonnet-Jegat, Flavien Bourdreux, Loïc Malet, Christian Serre, Marc Frere, Nathalie Steunou, J. Energy Storage, 2019, 25, 100881.
7 [vii] J Duan, W. Jin, S. Kitagawa, *Coord. Chem. Rev.*, 2017, **332**, 48-74.
8 [viii] X.-M. Liu, L-H. Xie, Y Wu, Inorg. Chem. Front., 2020, 7, 2840–2866
9 [ix] Schmidt, B. V. K. J. Metal-Organic Frameworks in Polymer Science: Polymerization Catalysis, Polymerization Environment, and Hybrid Materials. *Macromol. Rapid Commun.* **2020**, 41 (1), 1900333.
10 [x] Mark Kalaj, Kyle C. Bentz, Sergio Ayala, Jr., Joseph M. Palomba, Kyle S. Barcus, Yuji Katayama,Seth M. Cohen, Chem. Rev. 2020, 120, 8267–8302
11 [xi] Ma, K.; Idrees, K. B.; Son, F. A.; Maldonado, R.; Wasson, M. C.; Zhang, X.; Wang, X.; Shehayeb, E.; Merhi, A.; Kaafarani, B. R.; Islamoglu, T.; Xin, J. H.; Farha, O. K. Fiber Composites of Metal–Organic Frameworks. *Chem. Mater.* **2020**, 32 (17), 7120–7140.
12 [xii] Ali Saad, Subharanjan Biswas, Effrosyni Gkaniatsou, Clémence Sicard, Eddy Dumas, Nicolas Menguy,Nathalie Steunou, Chem. Mater. 2021, 33, 5825–5849
13 [xiii] Muschi, M.; Lalitha, A.; Sene, S.; Aureau, D.; Fregnaux, M.; Esteve, I.; Rivier, L.; Ramsahye, N.; Devautour-Vinot, S.; Sicard, C.; Menguy, N.; Serre, C.; Maurin, G.; Steunou, N. Formation of a Single-Crystal Aluminum-Based MOF Nanowire with Graphene Oxide Nanoscrolls as Structure-Directing Agents. *Angew. Chem. Int. Ed.* **2020**, 59 (26), 10353–10358.
14 [xiv] Benzaqui, M.; Semino, R.; Carn, F.; Tavares, S. R.; Menguy, N.; Giménez-Marqués, M.; Bellido, E.; Horcajada, P.; Berthelot, T.; Kuzminova, A. I.; Dmitrenko, M. E.; Penkova, A. V.; Roizard, D.; Serre, C.; Maurin, G.; Steunou, N. Covalent and Selective Grafting of Polyethylene Glycol Brushes at the Surface of ZIF-8 for the Processing of Membranes for Pervaporation. *ACS Sustain. Chem. Eng.* **2019**, 7 (7), 6629–6639.
15 [xv]

16 [xvi] C. Li, J. Liu, K. Zhang, S. Zhang, Y. Lee, T. Li, Angew. Chem. Int. Ed. 2021, 60, 14138-14145.
17 [xvii] D. Dai, H. Wang, C. Li, X. Qin, T. Li, *Angewandte Chemie International Edition* **2021**, *60*, 7389-7396

18

xviii A. Zimpel, T. Preiss, R. Roder, H. Engelke, M. Ingrisch, M. Peller, J. O. Radler, E. Wagner, T. Bein, U. Lachelt and S. Wuttke, *Chem. Mater.*, 2016, **28**, 3318-3326.

19 xix J. Lim, E. J. Lee, J. S. Choi, N. C. Jeong, *ACS applied materials interfaces* **2018**, *10*, 3793-3800

20 xx Y. Liu, C. S. Gong, C. Dai, Z. Yang, G. Yu, Y. Liu, M. Zhang, L. Lin, W. Tang, Z. Zhou, *Biomaterials* **2019**, *218*, 119365

21

xxi X. Zhu, H. Qiu, P. Chen, G. Chen and W. Min, *Carbon*, 2021, **176**, 530-539.

22 xxii Zhenjie Zhang, Ha Thi Hoang Nguyen, Stephen A. Miller, and Seth M. Cohen Angew. Chem. Int. Ed. 2015, 54, 6152 –6157

23 xxiii Jasmina Hafizovic Cavka, Søren Jakobsen, Unni Olsbye, Nathalie Guillou, Carlo Lamberti, Silvia Bordiga, and Karl Petter Lillerud, J. Am. Chem. Soc. **2008**, *130*, 13850–13851

24 xxiv Jonker, A. M., Löwik, D. W. P. M., van Hest, J. C. M., Peptide- and protein-based hydrogels. *Chem. Mater.*, 24, 759, 2012.

25 xxv N. Steunou, Advanced Materials Interfaces, 2016, 275-324.

26 xxvi Utech, S., Boccaccini, A. R., A review of hydrogel-based composites for biomedical applications: enhancement of hydrogel properties by addition of rigid inorganic fillers. *J. Mater. Sci.*, 51, 271, 2016.

27 xxvii Cölfen, H. Bio-Inspired Mineralization Using Hydrophilic Polymers. In *Biomineralization II: Mineralization Using Synthetic Polymers and Templates*; Naka, K., Ed.; Springer Berlin Heidelberg: Berlin, Heidelberg, 2007; pp 1–77.

28 xxviii Ashesh Garai, William Shepherd, Jia Huo and Darren Bradshaw, J. Mater. Chem. B, 2013, 1, 3678–3684

29 xxix Veis, A. et Aranyi, C., Phase separation in polyelectrolyte systems. I. Complex coacervates of gelatin. *J. Phys. Chem.*, 64, 1203, 1960.

30 xxx L.T. Gibson *et al*, *Corros. Sci.* **2010**, *52*, 172.link

31 xxxi A.-L. Dupont *et al*, *Studies in Conservation* **2000**, *45*, 201-210link

32 xxxii Al Mohtar, A., Nunes, S., Silva, J., Ramos, A. M., Lopes, J., & Pinto, M. L. (2021). *First-Principles Model to Evaluate Quantitatively the Long-Life Behavior of Cellulose Acetate Polymers*. ACS omega, 6(12), 8028-8037.

33 xxxiii Al Mohtar, Abeer, Moisés L. Pinto, Artur Neves, Sofia Nunes, Daniele Zappi, Gabriele Varani, Ana Maria Ramos et al. "*Decision making based on hybrid modeling approach applied to cellulose acetate based historical films conservation*." Scientific Reports 11, no. 1 (2021): 1-13.

34 xxxiv A. J. Cruz *et al*, *J. Chem. Eng. Data.* **2004**, *49*, 725.link

35 xxxv Kevin Dedecker, Renjith S. Pillai, Farid Nouar, Joao Pires,˜ Nathalie Steunou, Eddy Dumas, Guillaume Maurin, Christian Serre, Moises L. Pinto, ACS Appl. Mater. Interfaces 2018, 10, 13886–13894

36 xxxvi **Shyam Biswas,** *Eur. J. Inorg. Chem.* **2013**, 2154–2160

37 xxxvii Zhigang Hu, Inorg. Chem. 2015, 54, 4862–4868, DOI: 10.1021/acs.inorgchem.5b00435

38 xxxviii H. Furukawa, J. Am. Chem. Soc. 2014, 136, 4369–4381, 10.1021/ja500330a

39 xxxix Paul Iacomi, Chem. Mater. 2019, 31, 8413–8423, DOI: 10.1021/acs.chemmater.9b02322

40 xl J Choi,*J. Phys. Chem. C* 2018, 122, 10, 5545–5552

41 xli M. R. DeStefano, T. Islamoglu, S. J. Garibay, J. T. Hupp, O. K. Farha, *Chem. Mater.* **2017**, *29*, 1357-1361.

42 xlii A. Schaate, Chem. Eur. J. 2011, 17, 6643 – 6651

43 xliii Wenlong Xiang, J. Mater. Chem. A, 2020, 8, 21526–21546, 10.1039/d0ta08009h

44 xliv Francesca C. N. Firth, J. Mater. Chem. A, 2019, 7, 7459–7469, 10.1039/c8ta10682g

45 xlv Frederik Vermoortele, J. Am. Chem. Soc. 2013, 135, 11465–11468, dx.doi.org/10.1021/ja405078u |

46 xlvi G. C. Shearer, S. Chavan, S. Bordiga, S. Svelle, U. Olsbye, K. P. Lillerud, Chem. Mater. 28, 3749-3761.

47 xlvii G. C. Shearer, J. G. Vitillo, S. Bordiga, S. Svelle, U. Olsbye, K. P. Lillerud, Chem. Mater. 28, 7190-7193.

48 xlviii Y. Kondo, Y. Kuwahara, K. Mori, H. Yamashita, J. Phys.Chem. C, 2021, 125, 27909-27918

49 xlix Xiao Feng, ACS Appl. Mater. Interfaces 2021, 13, 60715–60735 https://doi.org/10.1021/acsami.1c13525

50 l Z. Chen, Langmuir 2018, 34, 14546–14551, 10.1021/acs.langmuir.8b03085

51 li B. Gibbons, E. C. Bartlett, M. Cai, X. Yang, E. M. Johnson, A. J. Morris, *Inorg. Chem* **2021**, *60*, 16378-16387.

52 lii P. G. Mileo, K. H. Cho, J. -S. Chang, G. Maurin, dalton Trans, 2021, 50, 1324-1333

53 liii Joly-Duhamel, C., Hellio, D., Djabourov, M., All gelatin networks: 1. Biodiversity and physical chemistry. *Langmuir,* 18, 7208, 2002

54 liv Bungenberg de Jong, H. G., Crystallisation-coacervation-flocculation, in : *Colloid Science*, H. G. Kruyt (Ed.), vol. 2, pp. 232-258, Elsevier, Amsterdam, 1949.

55 lv Florent Carn,a Nathalie Steunou, Madeleine Djabourov, Thibaud Coradin, François Ribot, Jacques Livage, Soft Matter, 2008, 4, 735–738

56 lvi Saeed Ahmad Khan, Marc Schneider, Macromol. Biosci. 2013, 13, 455–463

57 lvii Carn, F., Durupthy, O., Fayolle, B., Coradin, T., Mosser, G., Schmutz, M., Maquet, J., Livage, J., Steunou, N., Assembling vanadium (V) oxide and gelatin into novel bionanocomposites with unexpected rubber-like properties. *Chem. Mater. 22*, 398, 2010.

58 lviii Baroudi I., Simonnet-Jégat, C., Roch-Marchal, C., Leclerc-Laronze, N., Livage, C., Martineau C., Gervais C., Cadot, E., Carn F., Fayolle B., Steunou N., Supramolecular assembly of gelatin and inorganic polyanions: fine tuning the mechanical properties of nanocomposites by varying their composition and microstructure, *Chem. Mater.,* 27, 1452, 2015.

59 lix Coppola, M.; Djabourov, M.; Ferrand, M. Polymer 2012, 53,1483.

60 lx Gelse, K., Pöschl E., Aigner,T., Collagens-structure, function and biosynthesis. *Adv. Drug. Deliv. Rev.*, 55, 1531, 2003.

61 lxi R. Semino, J. C. Moreton, N. A. Ramsahye, S. M. Cohen, G. Maurin, *Chem. Sci.*, 2018,**9**, 315-324

62 lxii   Hwang, J.; Heil, T.; Antonietti, M.; Schmidt, B. V. K. J. Morphogenesis of Metal–Organic Mesocrystals Mediated by Double Hydrophilic Block Copolymers. *J. Am. Chem. Soc.* **2018**, 140 (8), 2947–2956.

63 lxiii Ross S. Forgan, Chem. Sci., 2020, 11, 4546–4562.

64 [lxiv] C. R. Marshall, S. A. Saudhammer, C. K. Brozek, Chem. Sci. 2019, 10, 9396-9408.
65 [lxv] R. J. Marshall, J. Mater Chem A, 2016, 4, 6955. 10.1039/c5ta10401g
66 [lxvi] Vincent J. Pastore, Timothy R. Cook, and Javid Rzayev, Chem. Mater. 2018, 30, 8639–8649